Use of the Field-Iteration Method in Studying the Three-Dimensional Phased Array for Electromagnetic Hyperthermia

Tianquan Deng

Abstract—**The field-iteration method (FIM) is used for simulation of the three-dimensional (3-D) phased array for deep regional hyperthermia at a frequency of 200 MHz. The iterative equation involving the electric field integral equation is derived using the dyadic Green's function with singularities at source points. The electric field and specific absorption rate distributions in a circular cylindrical model of muscle-like medium and in a model of computerized tomography scans of a liver cancer patient are calculated, respectively, using different amplitudes and/or phases and/or positions of individual applicators of the H-horn phased array. The obtained numerical results compared with the moment method results are analyzed to assess the accuracy of the field-iteration method and also to predict the advantages of the 3-D phased array hyperthermia system.**

I. Introduction

INTEREST IN using electromagnetic (EM) hyperthermia for cancer treatment has increased significantly [1]–[4]. Particularly in noninvasive EM hyperthermia, one attempts to focus the EM energy in the tumor, while avoiding damage the surrounding healthy tissue. The annular phased array (APA) is widely applied to such selectively localized heating because of its capability of steering the peak of the electric field by manipulating the amplitude and phase of the individual applicators [5]–[7]. Such a conventional APA hyperthermia system has obtained significant energy focus mainly on the plane where the applicators are placed, that is two-dimensional (2-D) EM-focus phased array (2-D-PA). In this paper, a three-dimensional (3-D) EM-focus phased array (3-D-PA) will be presented, in which each applicator can be arranged either in a planar or in annular or in a spherical array or any other array, for example, subannular and subspherical forms. A deionized water-loaded H-plane horn antenna is used as an element of such a phased array. This is because such a horn antenna phased array is characterized by good impedance matching between the patient and the horns. It also provides numerous selections of shifting the heating patterns by electrically varying the amplitude and/or the phase of the sources and/or manually changing the positions of the applicators. The H-horn applicator design and the 2-D simulations have been presented earlier [8] and [9].

Manuscript received September 26, 1995; revised February 13, 1996.

The author is with the National University of Singapore (NUS), Department of Electrical Engineering, Singapore.

Publisher Item Identifier S 0018-9480(96)07024-X.

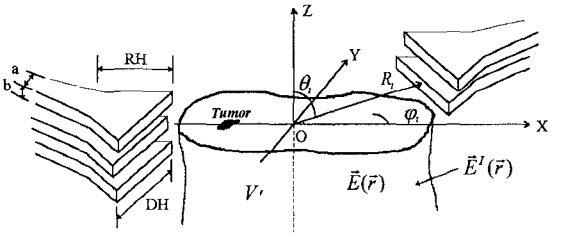

Fig. 1. 3-D H-horn phased device and its coordinates system.

In EM hyperthermia, computer simulation is a fast and convenient approach for device evaluation or for anticipating the effectiveness of a treatment. From the EM theory, this problem is EM scattering involving the electric field integral equation (EFIE) which contains a dyadic Green's function with the singularity at source points [10]–[12]. The conventional method of solving such a 2- or 3-D problem is to use the moment method (MM) [13] and [14]. In recent years, many other numerical methods, for example, FDTD [15], conjugate gradient method [16], hybrid boundary element method [17], etc., have been developed for solving electromagnetic scattering by inhomogeneous scatterers. The possibility and the validity of using an iterative method for electromagnetic scattering by some simple inhomogeneous models have been investigated recently [18] because of its computational efficiency and rapid convergence. A similar iteration method has been adopted by G. A. Thiele *et al.* [19]–[21] to solve the magnetic field integral equation (MFIE) and the electric field integral equation (EFIE) for scattering of a perfectly conducting body illuminated by a plane wave. In the present paper, we will concentrate on solving the 3-D electric field integral equation (EFIE) inside a volume of an irregularly shaped inhomogeneous dielectric body induced by arbitrary incident waves.

This iterative technique is used to solve the EFIE for two models in this paper. First, the calculation of a finite length cylinder of muscle-like medium illuminated by the phased array is analyzed to compare with its moment method results and to show the capability of shifting the E-field distributions. Second, a model based on CT scans of a liver cancer patient is simulated three-dimensionally in the case of different radiation conditions from the H-Horn phased array at a frequency of 200 MHz. It is shown that this iterative method does not involve the inversion of matrices and only requires a straightforward iteration procedure that is suitable for computer programming.

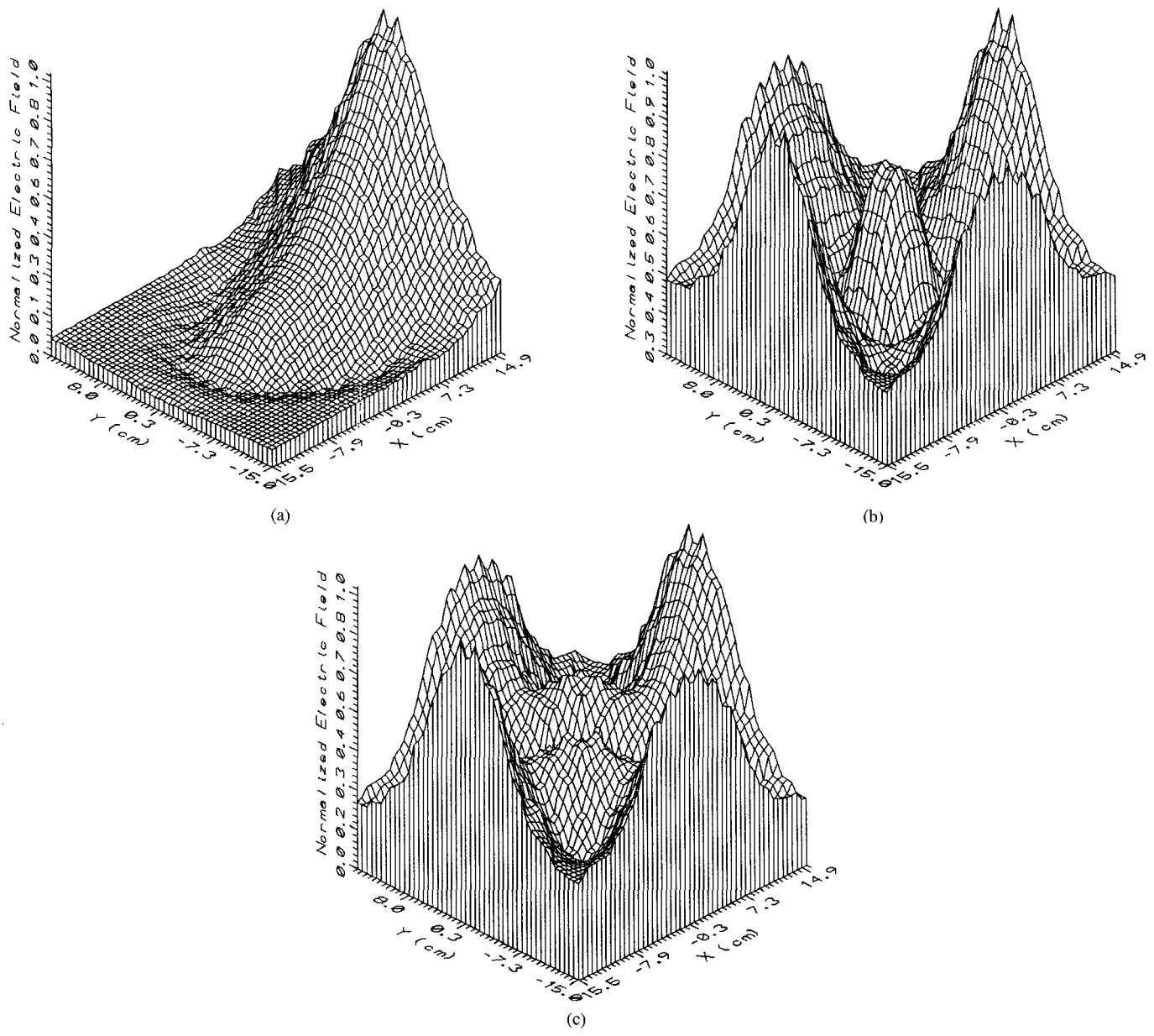

Fig. 2. The normalized E-field distributions on the central plane (XOY plane) of the muscle-like cylinder with three different radiation conditions: (a) one applicator positioned at $(R, \theta, \varphi) = (30\text{ cm}, 90°, 0°)$, (b) four applicators positioned at (30 cm, 90°, 0°), (30 cm, 90°, 90°), (30 cm, 90°, 180°), (30 cm, 90°, 270°) with equal amplitude and equal phase, and (c) four applicators placed at the same positions as (b), with equal amplitude on all applicators but with 180° phase lags on the applicators (30 cm, 90°, 180°) and (30 cm, 90°, 270°).

The effectiveness of the 3-D phased array hyperthermia system will also be discussed using the numerical results obtained.

II. Theory

In the following analysis, a $\exp(j\omega t)$ time dependence is assumed for field quantities, and the relative magnetic permeability in the media $\mu_r = 1$.

A. The Electric Field Integral Equation (EFIE)

Fig. 1 shows a 3-D arbitrarily-shaped inhomogeneous dielectric body (such as a human body) illuminated by an incident wave denoted by $\vec{E}^I(\vec{r})$. The incident field penetrates the dielectric body to produce the electric field denoted by $\vec{E}(\vec{r})$. By invoking the equivalence principle [22], we replace the dielectric body by the volume polarization current $\vec{J}_P(\vec{r}')$. Hence the total electric field inside the dielectric body V' can be expressed as

$$\vec{E}(\vec{r}) = \vec{E}^I(\vec{r}) + \iiint_{V'} j\omega\mu_0 \vec{J}_P(\vec{r}') \cdot \overline{\overline{G}}(\vec{r}, \vec{r}')\, dV' \qquad (1)$$

where $\vec{J}_P(\vec{r}')$ is the volume polarization current

$$\vec{J}_P(\vec{r}') = j\omega\varepsilon_0[\varepsilon_r(\vec{r}') - 1]\vec{E}(\vec{r}') \qquad (2)$$

and $\overline{\overline{G}}(\vec{r}, \vec{r}')$ is the electric dyadic Green's function in the source region [10]–[12]

$$\overline{\overline{G}}(\vec{r}, \vec{r}') = PV\overline{\overline{G_0}}(\vec{r}, \vec{r}') + \frac{\overline{\overline{L}}}{k_0^2}\,\delta(\vec{r} - \vec{r}'). \qquad (3)$$

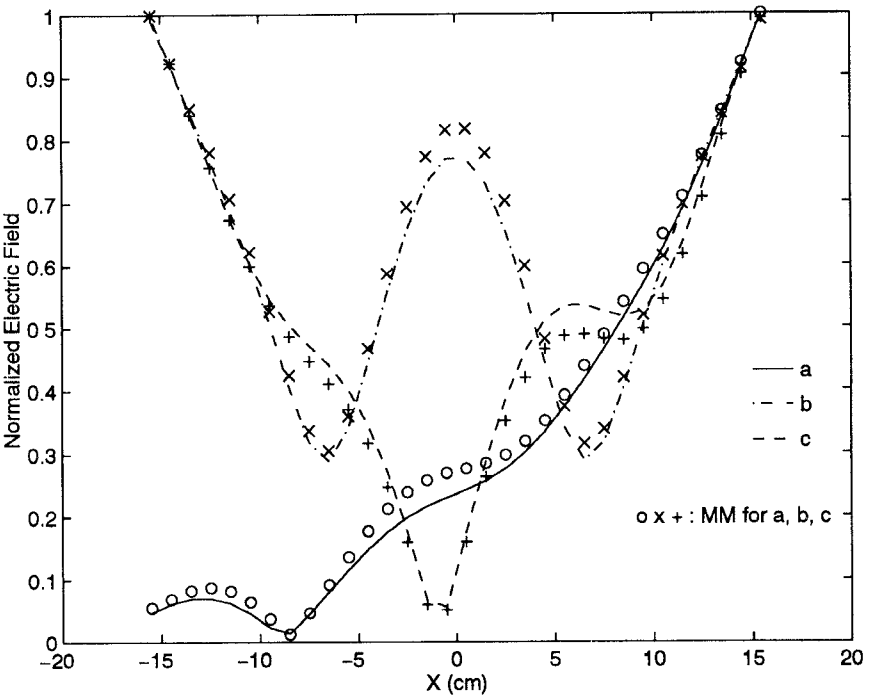

Fig. 3. The normalized E-field distributions along a diameter (X axis) corresponding to the three cases of Fig. 2.

PV denotes the principal value of the integral when the singularity appears in the source region [10]–[12]. $\overline{\overline{G_0}}(\vec{r}, \vec{r}')$ is the free-space dyadic Green's function, and $\overline{\overline{L}}$ is the depolarizing dyadic defined in [12]

$$\overline{\overline{G_0}}(\vec{r}, \vec{r}') = -\frac{1}{4\pi}\left(\overline{\overline{I}} + \frac{\nabla\nabla}{k_0^2}\right)\frac{\exp(-jk_0|\vec{r}-\vec{r}'|)}{|\vec{r}-\vec{r}'|} \tag{4}$$

$$\overline{\overline{L}} = \frac{\overline{\overline{I}}}{3}, \quad \text{when the principal volume is a sphere or a cube.} \tag{5}$$

Therefore, (1) can be rewritten as

$$\frac{\varepsilon_r(\vec{r})+2}{3}\vec{E}(\vec{r}) - \frac{k_0^2}{4\pi}PV\iiint_{V'}[\varepsilon_r(\vec{r}')-1]\vec{E}(\vec{r}') \cdot \left(\overline{\overline{I}} + \frac{\nabla\nabla}{k_0^2}\right)\frac{\exp(-jk_0|\vec{r}-\vec{r}'|)}{|\vec{r}-\vec{r}'|}\,dV' = \vec{E}^I(\vec{r}). \tag{6}$$

That is

$$\vec{E}(\vec{r}) = \frac{3}{\varepsilon_r(\vec{r})+2}\left\{\vec{E}^I(\vec{r}) + \frac{k_0^2}{4\pi}PV\iiint_{V'}[\varepsilon_r(\vec{r}')-1] \cdot \vec{E}(\vec{r}')\left(\overline{\overline{I}} + \frac{\nabla\nabla}{k_0^2}\right)\frac{\exp(-jk_0|\vec{r}-\vec{r}'|)}{|\vec{r}-\vec{r}'|}\,dV'\right\}. \tag{7}$$

Here

the hat "$\rightarrow$"	Denotes a vector.
the hat " $=$"	Denotes a dyadic.
$\vec{r}$	The position vectors at the field points.
$\vec{r}'$	The position vectors at the source points.
$\varepsilon_r(\vec{r})$	The relative complex permittivity.
$k_0 = \omega\sqrt{\varepsilon_0\mu_0}$	The free-space wave number.
$\overline{\overline{I}}$	The identity dyadic.

Equation (6) or (7) is the general formula for solution of scattering by an arbitrarily shaped inhomogeneous dielectric body. Equation (6) is the conventional expression that is solved by the moment method [13] and [14]. Equation (7) is a convenient form for the iterative procedure discussed in the following.

B. Iteration Method

In the (X, Y, Z) rectangular coordinates system the volume V' is divided into N subvolume cells, $\Delta V_n = 2a_n \cdot 2b_n \cdot 2c_n$, $n = 1, 2, \cdots, N$, where $2a_n$, $2b_n$, $2c_n$ are the distances along the X, Y, Z axes, respectively. The field and permittivity in each cell are assumed to be constant. Hence (7) can be discretized for each cell.

It is known that (7) is the Fredholm integral equation of the second kind [23], [24] which can be solved using iterative method. The procedure of the iterative method is as follows: substituting the incident field $\vec{E}^I(\vec{r}')$ as the initial solution into the right side of (7) to replace $\vec{E}(\vec{r}')$, we obtain a new field solution at the left side denoted by $\vec{E}^{(1)}(\vec{r})$; then substituting $\vec{E}^{(1)}(\vec{r})$ into the right side of (7) again, we obtain another solution $\vec{E}^{(2)}(\vec{r})$ at the left side; and so on, we get $\vec{E}^I \rightarrow \vec{E}^{(1)} \rightarrow \vec{E}^{(2)} \rightarrow \cdots \rightarrow \vec{E}^{(l-1)} \rightarrow \vec{E}^{(l)}$, that is

$$E_x^{(l)}(m) = \frac{3}{\varepsilon_r(m)+2}\left\{E_x^I(m) + \sum_{n=1}^{N}\frac{\varepsilon_r(n)-1}{4\pi} \cdot ([Q_{yy}(m,n) + Q_{zz}(m,n)]E_x^{(l-1)}(n) + Q_{xy}(m,n)E_y^{(l-1)}(n) + Q_{xz}(m,n)E_z^{(l-1)}(n))\right\} \tag{8}$$

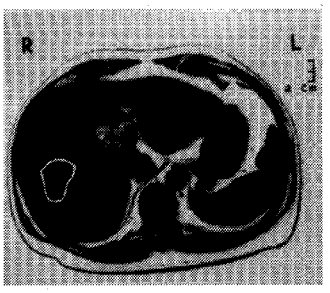

(a)

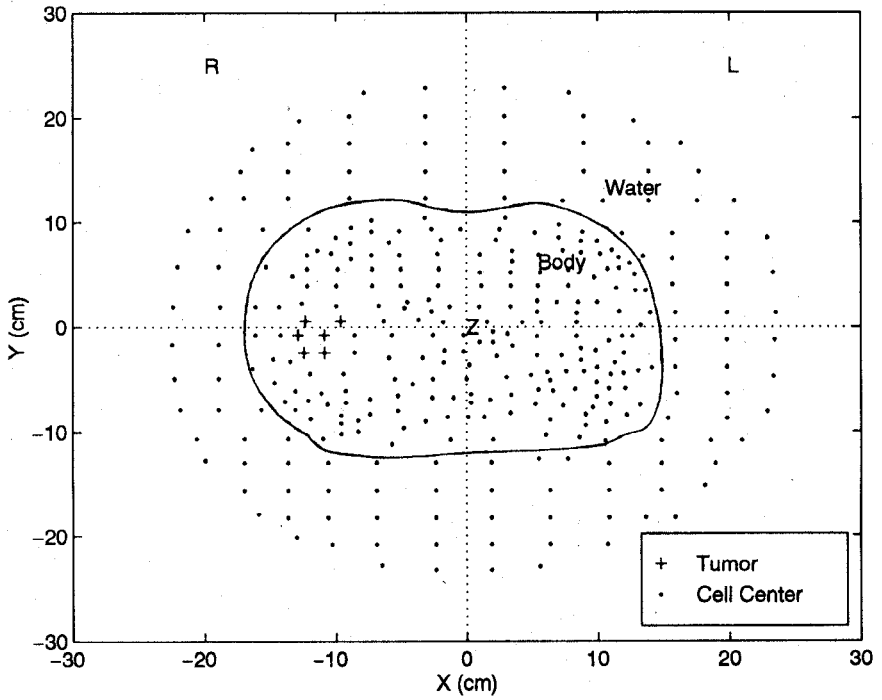

(b)

Fig. 4. (a) Computerized tomography (CT) scan of a liver cancer body with the tumor region encircled. (b) The discretized version of the above CT scan.

$$E_y^{(l)}(m) = \frac{3}{\varepsilon_r(m)+2}\left\{E_y^I(m) + \sum_{n=1}^{N}\frac{\varepsilon_r(n)-1}{4\pi} \cdot \left(Q_{yx}(m,n)E_x^{(l-1)}(n) + [Q_{xx}(m,n)+Q_{zz}(m,n)] \cdot E_y^{(l-1)}(n) + Q_{yz}(m,n)E_z^{(l-1)}(n)\right)\right\} \quad (9)$$

$$E_z^{(l)}(m) = \frac{3}{\varepsilon_r(m)+2}\left\{E_z^I(m) + \sum_{n=1}^{N}\frac{\varepsilon_r(n)-1}{4\pi} \cdot \left(Q_{zx}(m,n)E_x^{(l-1)}(n) + Q_{zy}(m,n)E_y^{(l-1)}(n) + [Q_{xx}(m,n)+Q_{yy}(m,n)]E_z^{(l-1)}(n)\right)\right\} \quad (10)$$

where

$m, n = 1, 2, \cdots, N;\ l = 1, 2, \cdots$

$(m) = (\vec{r}_m) = (x_m, y_m, z_m)$ The coordinates at the field points.

$(n) = (\vec{r}'_n) = (x'_n, y'_n, z'_n)$ The coordinates at the source points.

$\varepsilon_r(m)$ The relative complex permittivity of cell m.

$E_x^{(l-1)}(m)$ The x component of electric field in the cell m after $l$steps of iterations.

$Q_{st}(m,n)|_{s,t=x,y,z}$ The coupling coefficients between cell m and cell n given in the following.

1) If $m = n$, i.e., $(x_m, y_m, z_m) = (x'_n, y'_n, z'_n)$, we have

$$Q_{xx}(m,n) = 4\pi\left\{\frac{a_n}{L_1}\exp(-jk_0L_1) - \exp(-jk_0a_n) + \frac{1}{3}\right\} + 16a_n\int_0^{\pi/4}\left\{\frac{1}{L_2}\exp(-jk_0L_2) - \frac{1}{L_1}\exp(-jk_0L_1)\right\}d\varphi' + 8a_n\int_0^{\tan^{-1}(c_n/b_n)}\left\{\frac{1}{L_3}\exp(-jk_0L_3)\right.$$

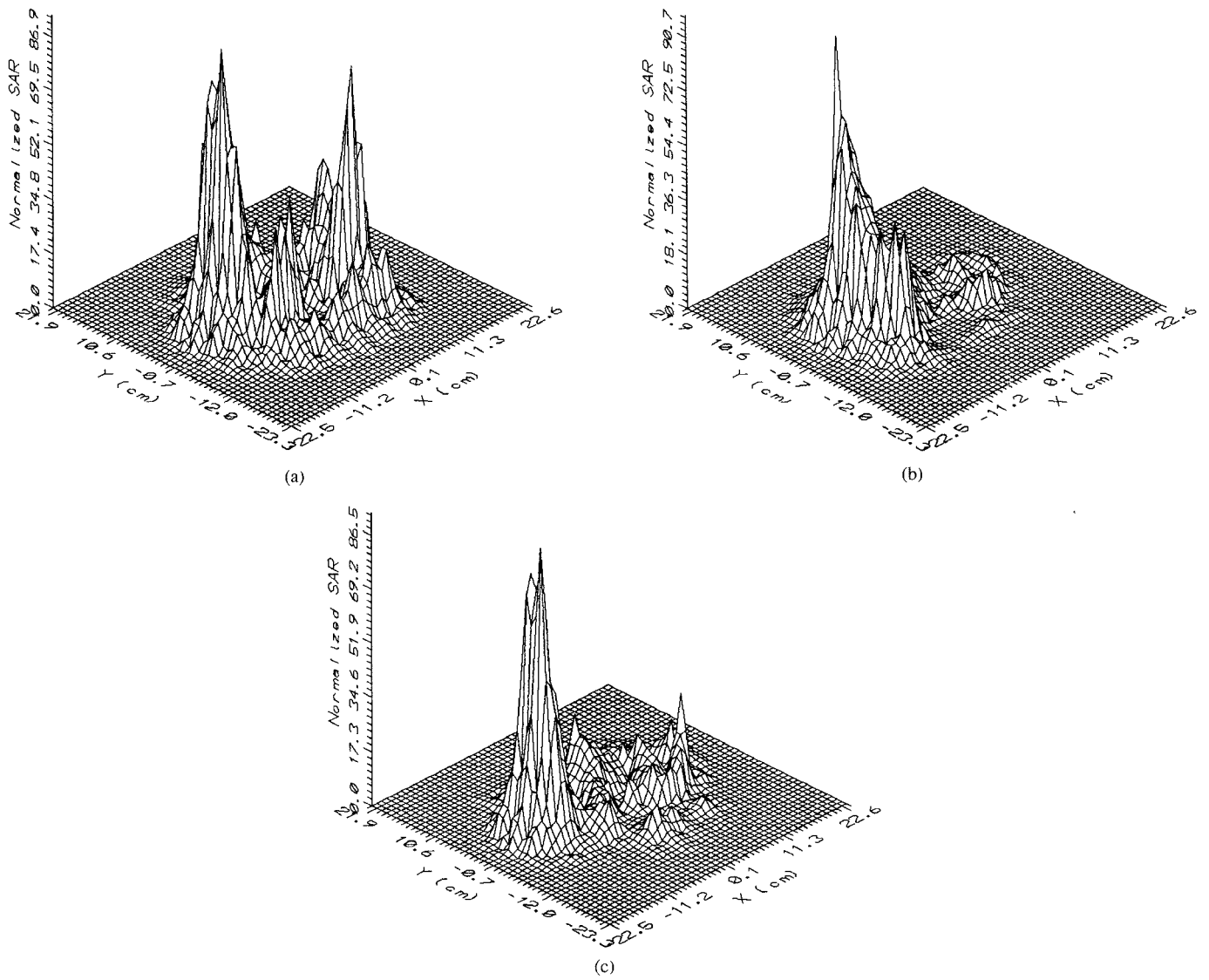

Fig. 5. The normalized SAR distributions on the XOY plane under three different radiation conditions at 200 MHz: (a) six horn antennas placed uniformly and annularly around the model with equal amplitude and phase on each antenna. (b) three horn antennas positioned at (30 cm, 90°, 90°), (30 cm, 90°, 135°), (30 cm, 90°, 180°) with equal amplitude and equal phase on each antenna, and (c) nine horn antennas to form a 3-D phased array with 3-row and 3-column horns positioned at (26.5 cm, 70°, 135°), (30 cm, 90°, 135°), (26.5 cm, 110°, 135°); (26.5 cm, 70°, 180°), (30 cm, 90°, 180°), (26.5 cm, 110°, 180°); (26.5 cm, 70°, 225°), (30 cm, 90°, 225°), (26.5 cm, 110°, 225°), energized, respectively, in amplitudes of 3×0.6, 3×1.0, 3×0.6 and in phases lags of $3\times0°$, $3\times70°$, $3\times0°$.

$$-\frac{1}{L_2}\exp(-jk_0L_2)\Bigg\}d\varphi' + 8a_n\int_{\tan^{-1}(c_n/b_n)}^{\pi/4}\Bigg\{\frac{1}{L_4}\exp(-jk_0L_4) - \frac{1}{L_2}\exp(-jk_0L_2)\Bigg\}d\varphi' \tag{11}$$

where

$$L_1 = \sqrt{a_n^2 + c_n^2}$$

$$L_2 = \sqrt{a_n^2 + \left(\frac{c_n}{\cos\varphi'}\right)^2}$$

$$L_3 = \sqrt{a_n^2 + \left(\frac{b_n}{\cos\varphi'}\right)^2}$$

$$L_4 = \sqrt{a_n^2 + \left(\frac{c_n}{\sin\varphi'}\right)^2} \tag{12}$$

and

$$\begin{aligned} Q_{yy}(m,n) &= Q_{xx}(m,n)|_{a_n\leftrightarrow b_n} \\ Q_{zz}(m,n) &= Q_{xx}(m,n)|_{a_n\leftrightarrow c_n} \\ Q_{xy}(m,n) &= Q_{yx}(m,n) \\ &= 0 \\ Q_{zx}(m,n) &= Q_{xz}(m,n) \\ &= 0 \\ Q_{yz}(m,n) &= Q_{zy}(m,n) \\ &= 0. \end{aligned} \tag{13}$$

Here, the symbol "↔" means replacement.

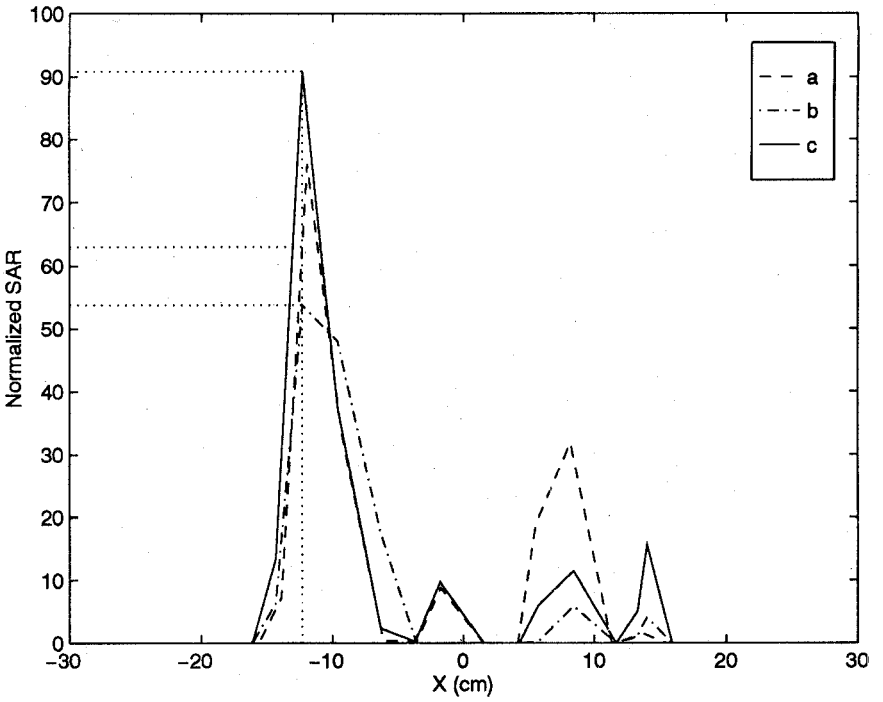

Fig. 6. Comparisons of the normalized SAR along the X axis going through the liver tumor for three cases of Fig. 5. The dotted lines indicate the position of the tumor center and the respective SAR values for each case.

2) If $m \neq n$, i.e., $(x_m, y_m, z_m) \neq (x'_n, y'_n, z'_n)$, we have

$$\begin{aligned} Q_{xx}(m,n) &= \int_{y'_n-b_n}^{y'_n+b_n}\int_{z'_n-c_n}^{z'_n+c_n} \cdot \left\{(x'_n - a_n - x_m)\frac{jk_0L_5+1}{(L_5)^3} \cdot \exp(-jk_0L_5) - (x'_n + a_n - x_m) \cdot \frac{jk_0L_6+1}{(L_6)^3}\exp(-jk_0L_6)\right\} dy'\,dz' \quad (14) \\ Q_{xy}(m,n) &= \int_{y'_n-b_n}^{y'_n+b_n}\int_{z'_n-c_n}^{z'_n+c_n} (y'_n - y_m) \cdot \left\{\frac{jk_0L_5+1}{(L_5)^3}\exp(-jk_0L_5) - \frac{jk_0L_6+1}{(L_6)^3}\exp(-jk_0L_6)\right\} dy'\,dz' \quad (15) \end{aligned}$$

where

$$\begin{aligned} L_5 &= \sqrt{(x'_n - a_n - x_m)^2 + (y' - y_m)^2 + (z' - z_m)^2} \\ L_6 &= \sqrt{(x'_n + a_n - x_m)^2 + (y' - y_m)^2 + (z' - z_m)^2}. \end{aligned} \quad (16)$$

The other forms of $Q_{st}(m, n)$ are similar and not given here. The convergence coefficient $g^{(l)}$ of the l step of iteration is defined as

$$g^{(l)} = \frac{1}{N}\sum_{m=1}^{N}\left\{\frac{|\vec{E}^{(l)}(m) - \vec{E}^{(l-1)}(m)|}{|\vec{E}^{(l)}(m)|}\right\}. \quad (17)$$

$g^{(l)}$ is a very important parameter to judge whether the iteration is convergent or not.

C. The Incident Field from the Phased Array

The incident field produced by 3-D H-horn phased array hyperthermia system (shown in Fig. 1) is

$$\vec{E}^I(\vec{r}) = \sum_i \vec{E}_i^I(\vec{r}). \quad (18)$$

$\vec{E}_i^I(\vec{r})$ is the radiation field from the horn antenna i

$$\vec{E}_i^I(\vec{r}) = A_i \iint_{S'}\left\{\vec{E}_{a,i}(\vec{r}')\frac{\partial}{\partial n'}\left[\frac{\exp(-jk_0|\vec{r}-\vec{r}'|)}{|\vec{r}-\vec{r}'|}\right]\right\} dS' \quad (19)$$

where $\vec{E}_{a,i}$ is the aperture E-field of the horn antenna i, it takes different forms for different kinds of aperture antennas, such as waveguide antenna and slot antenna etc.

In the (X, Y, Z) coordinates system shown in Fig. 1, for a H-horn phased array, the above radiation field can be expressed as

$$\vec{E}_i^I(x,y,z) = \hat{t}'A_i \int_{-DH/2}^{DH/2}\int_{-b/2}^{b/2} \cdot \left\{\cos\left(\frac{\pi x'}{DH}\right)\exp\left(\frac{-j\pi x'^2}{\lambda RH} - j\phi_i\right) \cdot \frac{\partial}{\partial n'}\left[\frac{\exp(-jk_0|\vec{r}-\vec{r}'|)}{|\vec{r}-\vec{r}'|}\right]\right\} dx'\,dz' \quad (20)$$

where

$$|\vec{r} - \vec{r}'| = \sqrt{(x_i - x')^2 + (y_i)^2 + (z_i - z')^2} \quad (21)$$

with

$$x_i = x\sin\varphi_i - y\cos\varphi_i - R_i\sin\theta_i\cos\varphi_i \quad (22)$$

$$y_i = x\sin\theta_i\cos\varphi_i + y\sin\theta_i\sin\varphi_i + z\cos\theta_i - R_i\sin\theta_i\sin\varphi_i \quad (23)$$

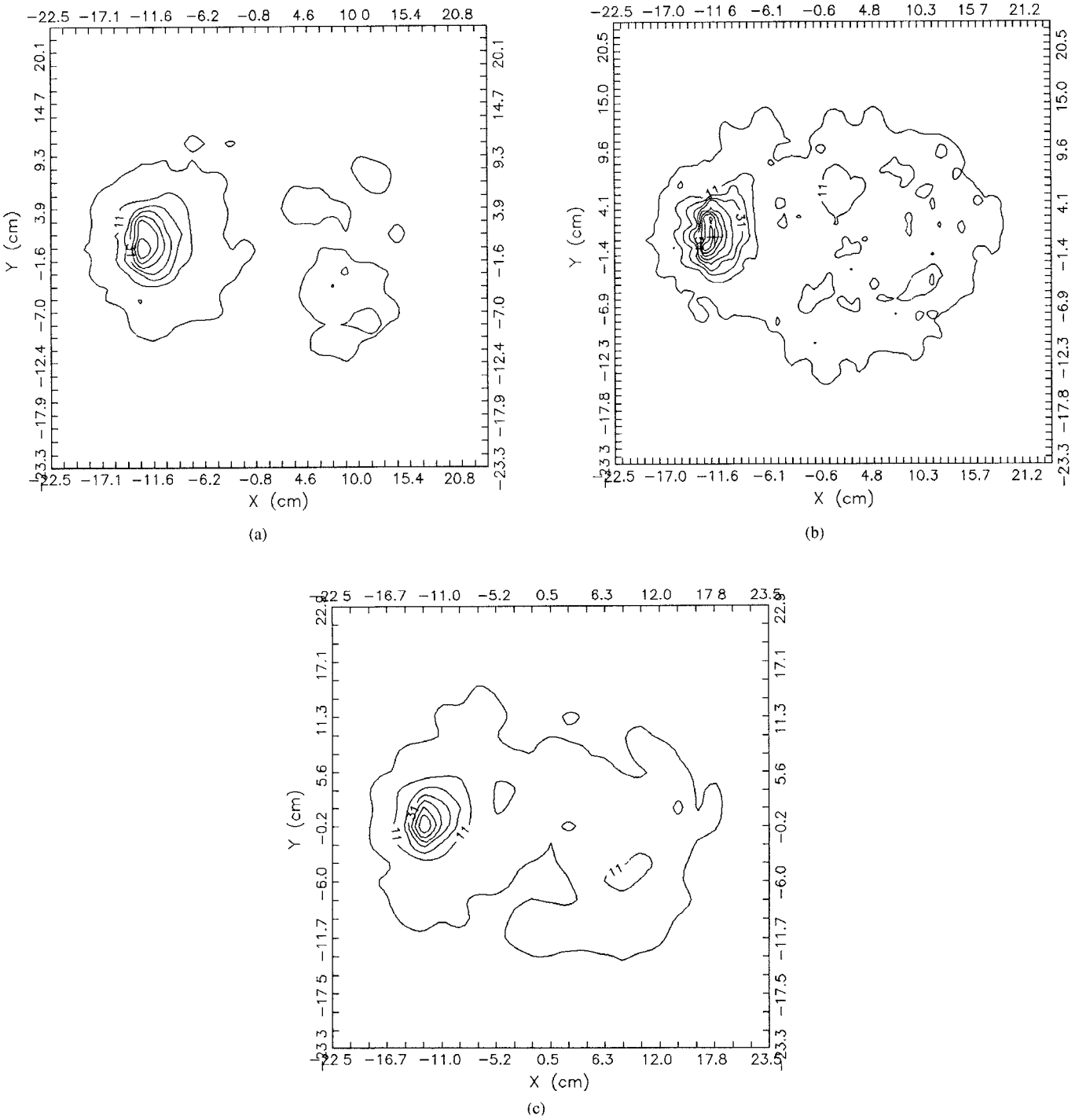

Fig. 7. Comparisons of the normalized SAR along the Z direction in the optimized case. Contour (a) on the plane $Z = -2.5$ cm; Contour (b) on the plane $Z = 0$ cm (in which "+" denotes the location of the tumor); and Contour (c) on the plane $Z = 2.5$ cm.

$$z_i = -x\cos\theta_i\cos\varphi_i - y\cos\theta_i\sin\varphi_i + z\sin\theta_i - R_i\cos\theta_i. \tag{24}$$

$\hat{t}'$ and $\hat{n}'$ are the unit vectors, respectively, in the tangential and normal directions of the antenna aperture plane. RH, DH, and b are sizes of the horn antenna.λ is the wavelength at the operating frequency. R_i, θ_i, φ_i denote the position of antenna i. A_i, ϕ_i are the amplitude and phase of antenna i, respectively.

Here R_i, θ_i, φ_i and A_i, ϕ_i are used to control the electric field distributions produced by the phased array. Then the E-field can be used to calculate the specific absorption rate (SAR)

$$\text{SAR} = \frac{\frac{1}{2}\sigma|\vec{E}|^2}{\rho_m} = \frac{\pi\varepsilon_0\varepsilon'' f|\vec{E}|^2}{\rho_m} \tag{25}$$

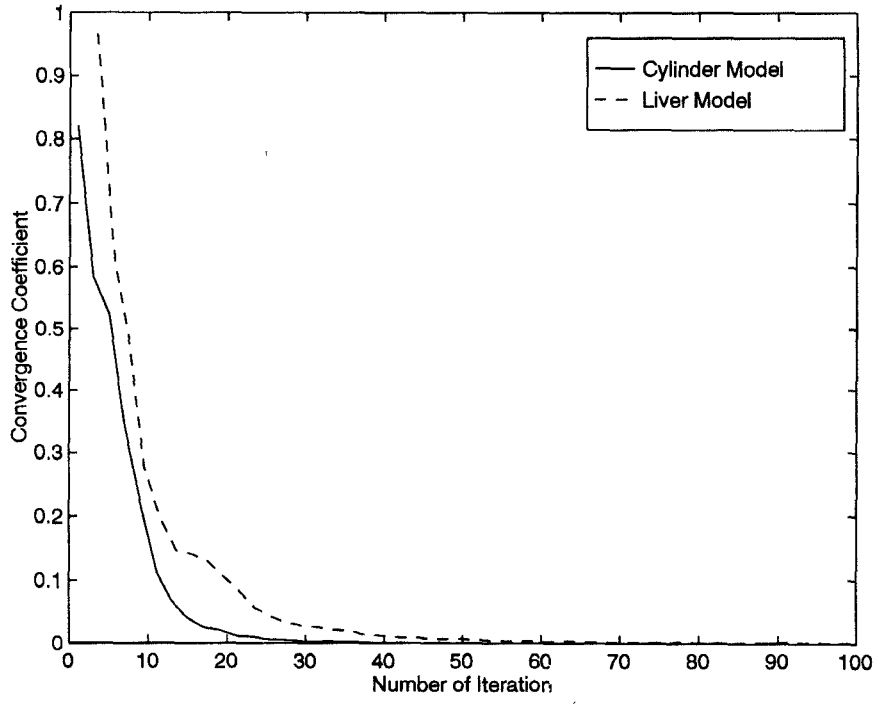

Fig. 8. The convergence coefficient versus the number of iteration.

where σ is the conductivity of the lossy dielectric media, ρ_m the density, ε'' the loss factor of tissue or dielectric objects, and f is the operating frequency.

III. Numerical Results

A. The Muscle-Like Cylinder Model

To understand the electrical energy focus and shifting ability of the H-horn phased array, and to assess the accuracy of the field-iteration method, the E-field distributions inside a circular cylindrical model of muscle-like medium are calculated under several different radiation conditions. The muscle-like medium has a complex permittivity $\varepsilon_r = 56 - j90$ at 200 MHz and a density $\rho_m = 1.02 \times 10^3$ kg/m^3. The applicators are placed on the central horizontal plane of the cylinder that has a diameter of 32 cm and a height of 80 cm. The entire cylindrical structure consists of 8064 cells with a cell size of less than 2 cm.

Fig. 2 shows the absolute normalized E-field distributions on the central plane (XOY plane shown in Fig. 1) of the whole radiation space surrounded by the APA where the horn applicators are placed. The numerical results are obtained in three cases [shown in Fig. 2(a)–(c)]: (a) one applicator positioned at $(R, \theta, \varphi) = (30$ cm, 90°, 0°), (b) four applicators positioned at (30 cm, 90°, 0°), (30 cm, 90°, 90°), (30 cm, 90°, 180°), (30 cm, 90°, 270°) with equal amplitude and equal phase, (c) four applicators placed at the same positions as (b), with equal amplitude on all applicators but with 180° phase lags on the applicators (30 cm, 90°, 180°) and (30 cm, 90°, 270°).

In order to compare with moment method (MM) results conveniently, more obviously 2-D curves are used to show the above E-field distributions along a diameter on the X-axis (Fig. 3). It is found that the FIM results agree very well with those from moment method (MM), and the CPU time of FIM code can be reduced by 20% compared with those of MM. It is shown that the E-field distributions shift significantly with changes in radiation conditions of the applicators.

B. The Model from CT Scans

A realistic model of a liver cancer patient irradiated by the H-horn phased array system is simulated to predict the specific absorption rate (SAR) inside the upper abdomen of the patient. The model simulated is based on computerized tomography (CT) scans along the axis of the body. Fig. 4(a) displays one such CT scans on the central plane of a $4 \times 5 \times 5$ cm^3 tumor encircled inside the patient's liver. Fifteen such CT slices taken from the last rib to the top of the diaphragm of the patient form the input data for simulations. In practice a deionized water bolus is typically used between the patient body and the radiation horns to improve field matching as well as to obtain superficial cooling. Therefore the simulated 3-D space consists of the filled water and the body itself. Normally the applicators are placed at the level of the liver cancer region. The whole model consists of 24 930 volume cells with different cell size of around 1 cm. The values for dielectric constants and densities of various tissues have been tabulated in the paper [25]. A rectangular coordinates system is established so that the X axis goes through the tumor, the Y axis goes from the back to the front of the patient body and Z axis goes along the axis of the body from the head to the feet. Fig. 4(b) presents the discretized version of the above CT scan, in which the position of each cell, the position and the dimensions of the tumor as well as the established coordinates system are shown precisely.

Fig. 5(a)–(c) shows the normalized SAR distributions on the XOY plane under three different radiation conditions at 200

MHz. The SAR values are normalized by their maxim 100 in each set of radiation conditions. Fig. 5(a) corresponds to the case of six horn antennas placed uniformly and annularly around the model with equal amplitude and phase on each antenna. Fig. 5(b) corresponds to the case of three horn antennas positioned at (30 cm, 90°, 90°), (30 cm, 90°, 135°), (30 cm, 90°, 180°) with equal amplitude and equal phase on each antenna. Fig. 5(c) corresponds to the optimized results with relatively high SAR value deposited in the tumor region. In this case, nine horn antennas are used to form a 3-D phased array with 3-row and 3-column horns positioned at (26.5 cm, 70°, 135°), (30 cm, 90°, 135°), (26.5 cm, 110°, 135°); (26.5 cm, 70°, 180°), (30 cm, 90°, 180°), (26.5 cm, 110°, 180°); (26.5 cm, 70°, 225°), (30 cm, 90°, 225°), (26.5 cm, 110°, 225°). These antennas are energized, respectively, in amplitudes of 3×0.6, 3×1.0, 3×0.6 and in phases lags of $3 \times 0°$, $3 \times 70°$, $3 \times 0°$. Because of computation expense, the optimization has been done by using good initial estimates and large steps in terms of the position and the amplitude and phase on each applicator. In order to understand the ability of the horn phased array hyperthermia system to focus the electric energy on the desired region such as the tumor region, the above three cases of the normalized SAR along the X axis going through the liver tumor are compared in Fig. 6. The dotted lines indicate the position of the tumor center and the respective SAR values for each case. Curves a, b, and c in Fig. 6 correspond to Fig. 5(a)–(c), respectively.

In Fig. 5(a), the desired heating pattern has not been obtained due to no any manipulation of the radiation parameters on the applicators. It is a simple and efficient way to shift the power pattern significantly only by adjusting the positions of the applicators [shown in Fig. 5(b)]. The desired selectively heating in tumors has been achieved in the case of Fig. 5(c) by optimizing SAR's to find the amplitudes and phases as well as the positions of the applicators. It is more obviously shown in Fig. 6 that up to 91 of SAR in cancers has been attained in curve c, while the SAR's are less than 65 in curve a and less than 55 in curve b. The normalized SAR values represent relatively the percentage of the absorbed power in each cell to the total power. Therefore, obviously case c [shown in Fig. 5(c) and curve c in Fig. 6] is the desired heating scheme for the liver cancer patient.

It has been pointed out that the presented 3-D phased array is capable of focusing EM energy in 3-D directions. Its focus feature along the X and Y directions has already been shown in Figs. 5 and 6. Moreover its focus capability along the Z direction is shown in Fig. 7 for the above optimized case. Contour (a) with maximum SAR of 65 is plotted on the plane $Z = -2.5$ cm (upper end of the tumor); Contour (b) with maximum SAR of 90 is on the plane $Z = 0$ cm (the tumor located); and Contour (c) with maximum SAR of 70 is on the plane $Z = 2.5$ cm (lower end of the tumor).

Each run of the FIM code for a set of radiation conditions requires 31–38 CPU min on a VAX-11/750 computer. Computations in this paper also demonstrate that the iterative method is efficient and accurate. It does not involve the inversion of matrices and direct boundary condition. The excellent numerical convergence behavior in Fig. 8 supports this feature, in which the convergence coefficient $g \leq 0.01$ is gotten after 40 iteration steps for curve a when the cylinder is modeled in the case of Fig. 2, and after 60 iteration steps for curve b when the human body model is calculated in the case of Fig. 5.

Based upon the presented performance of the FIM code, it shows promise as a fast and accurate method for numerically studying electromagnetic hyperthermia. As stated in the paper [19]–[21], the FIM code has the following advantages: it is extremely simple to write programs and execute rapidly; it does not involve the inversion of matrices; its numerical convergence is rapid.

IV. Conclusion

In this paper, a new iterative method is developed to compute the electric fields inside an arbitrarily shaped inhomogeneous dielectric body such as a human body. The validity and good accuracy of the field-iteration method (FIM) have been tested using the moment method. The feature of 3-D H-horn phased array hyperthermia system at 200 MHz suitable for heating deep-seated regional and eccentric cancers by manipulating the radiation parameters have been investigated. The technique developed in this paper can be easily applied to other phased array hyperthermia system and other locations of tumors in different patients.

Acknowledgment

The author is grateful to Dr. X. H. Zhang of Chengdu Army General Hospital for providing the CT scans and helpful discussions. The author would also like to thank the reviewers for helpful comments regarding the manuscript.

References

[1] Special issue on "Hyperthermia and cancer therapy," *IEEE Trans. Microwave Theory Tech.*, vol. MTT-34, 1986.

[2] T. Cetas, "Hyperthermic physics," in *Hyperthermic Oncology*, T. Sugahara and M. Satio, Eds. New York: Taylor & Francais, 1988/1989, pp. 24–29.

[3] M. Kikuchi, "Recent progress of electromagnetic techniques in hyperthermia treatment," *IECE Trans Comm.*, vol. E78-B, no. 6, pp. 799–808, 1995.

[4] S. L. Dvorak and D. J. Aziz, "Numerical analysis of printed strip dipole hyperthermia applicators," *IEEE Trans. Microwave Theory Tech.*, vol. 43, no. 7, pp. 1502–1507, 1995

[5] P. F. Turner, "Regional hyperthermia with an annular phased array," *IEEE Trans. Biomed. Eng.*, vol. BME-31, pp. 106–114, 1984.

[6] V. Sathiaseelan, M. F. Iskander, G. C. Howard, and N. M. Bleehen, "Theoretical analysis and clinical demonstration of the effect of power pattern control using the annular phased-array hyperthermia system," *IEEE Trans. Microwave Theory Tech.*, vol. MTT-34, pp. 514–519, 1986.

[7] Y. Zhang, W. T. Joines, R. L. Jirtle, and T. V. Samulski, "Theoretical and measured electric field distributions within an annular phased array: Consideration of source antenna," *IEEE Trans. Biomed. Eng.*, vol. 40, no. 8, pp. 780–787, 1993.

[8] T. Deng, "Optimization of SAR distributions in liver and lung regions irradiated by the H-horn annular phased array hyperthermia system," *IEEE Trans. Microwave Theory Tech.*, vol. 39, no. 5, pp. 852–856, 1991.

[9] T. Deng, Z. Liang, and W. Ren, "Theoretical analysis of H-horn annular phased array system for heating deep-seated tumors," *J. Microwave Power EM Energy*, vol. 26, pp. 100–106, 1991.

[10] J. V. Bladel, "Some remarks on Green's dyadic for infinite space," *IRE Trans. Antennas Propagat.*, vol. AP-9, pp. 563–566, 1961.

[11] S. W. Lee, J. Boersma, C. L. Law, and G. A. Deschamps, "Singularity in Green's function and its numerical evaluation," *IEEE Trans. Antennas Propagat.*, vol. AP-28, no. 3, pp. 311–317, 1980.

[12] A. D. Yaghjian, "Electric dyadic Green's functions in the source region," *Proc. IEEE*, vol. 68, no. 2, pp. 248–263, 1980.

[13] R. F. Harrington, *Field Computation by Moment Methods.* New York: MacMillan, 1968.
[14] D. E. Livesay and K. M. Chen, "Electromagnetic fields induced inside arbitrarily shaped biological bodies," *IEEE Trans. Microwave Theory Tech.,* vol. MTT-22, no. 12, pp. 1273–1280, 1974.
[15] A. Taflove, "Review of the formulation and applications of the finite-difference time-domain method for numerical modeling of the electromagnetic wave interactions with arbitrary structure," *Wave Motion,* vol. 10, no. 6, pp. 547–582, 1988.
[16] J. J. H. Wang and J. R. Dubberley, "Computation of fields in an arbitrarily shaped heterogeneous dielectric or biological body by an iterative conjugate gradient method," *IEEE Trans. Microwave Theory Tech.,* vol. 37, no. 7, pp. 1119–1125, 1989.
[17] K. D. Paulsen, D. R. Lynch, and J. W. Strobehn, "Three-dimensional finite, boundary and hybrid element solutions of the Maxwell equations for lossy dielectric media," *IEEE Trans. Microwave Theory Tech.,* vol. 36, no. 4, pp. 682–693, 1988.
[18] T. Deng and X. Liu, "Iterative solutions of three-dimensional electric fields and absorbed powers inside a human body illuminated by a horn-antenna annular phased array," in *Proc. Int. Symp. IEEE Antennas Propag. Society,* Newport Beach, CA, June, 1995, vol. 3, pp. 1573–1576.
[19] M. Kaye, P. K. Murthy, and G. A. Thiele, "An iterative method for solving scattering problems," *IEEE Trans. Antennas Propagat.,* vol. AP-33, no. 11, pp. 1272–1279, 1985.
[20] P. K. Murthy, K. C. Hill, and G. A. Thiele, "A hybrid-iterative method for scattering problems," *IEEE Trans. Antennas Propagat.,* vol. AP-34, no. 10, pp. 1173–1180, 1986.
[21] D. D. Reuster and G. A. Thiele, "A field iterative method for computing the scattered electric fields at the apertures of large perfectly conducting cavities," *IEEE Trans. Antennas Propagat.,* vol. 43, no. 3, pp. 286–290, 1995.
[22] R. F. Harrington, *Time-Harmonic Electromagnetic Fields.* New York: McGraw-Hill, 1961.
[23] W. Pogorzelski, *Integral Equations and Their Applications.* New York: Pergamon, 1966, vol. 1.
[24] M. A. Golberg, "A survey of numerical methods for integral equations," in *Solution Methods for Integral Equations—Theory and Appl.,* M. A. Golberg, Ed. New York: Plenum, 1978, pp. 1–58.
[25] M. A. Stuchly and S. S. Stuchly, "Dielectric properties of biological substances — Tabulated," *J. Microwave Power,* vol. 15, pp. 19–26, 1980.

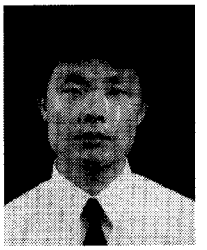

Tianquan Deng was born in Sichuan, China, in 1964. He received the B.S. degree in physics from Sichuan Normal University (SNU) in 1986, the M.S. degree in microwave electronics from the University of Electronic Science and Technology of China (UESTC) in 1988, and Ph.D. degree in electrical engineering from the National University of Singapore (NUS) in 1996.

Currently, he is a Research Scholar at NUS, working on CAD models and full-wave analysis of (M)MIC components and systems. He was a Research Engineer and Lecturer at UESTC from 1989 to 1994, where he built and headed Hongya Institute, and participated in establishing the High Power Microwave Lab. His main research work involved RF/microwave hyperthermia, high power microwave sources, and free electron lasers. His current research interests are in electromagnetic theory and biomedical applications, high power microwaves and millimeter waves, CAD models for hybrid and monolithic MIC's, RF circuits, antenna designs, and mobile communications. He has published more than 30 technical papers in the international journals and conferences in these areas.

He has been a reviewer for manuscripts from the *Journal of Heat Transfer of America,* has served on a committee of the National Institute of Microwave Biomedical Engineering, Beijing, and served as a Session Chairman of Asia-Pacific Microwave Conference'95, Korea. He is a member of AAAS and CIE, and has been selected for inclusion in the 14th *Who's Who in the World.*